

Quantum illumination with asymmetrically squeezed two-mode light

Yonggi Jo,* Taek Jeong, Junghyun Kim, Duk Y. Kim, Yong Sup Ihn, Zaeill Kim, and Su-Yong Lee†

*Quantum Physics Technology Directorate, Advanced Defense Technology Research Institute,
Agency for Defense Development, Yuseong P.O. Box 35, Daejeon 34186, Republic of Korea*

(Dated: March 1, 2025)

We propose a Gaussian quantum illumination(QI) protocol exploiting asymmetrically squeezed two-mode(ASTM) light that is generated by applying single-mode squeezing operations on each mode of the initial two-mode squeezed vacuum(TMSV) state. We show that the performance of our protocol can approach that of the conventional Gaussian QI with the same probe energy under certain conditions, when we have an obstacle of attaining a bright TMSV state. Additionally, an ASTM state provides a counterexample of the previously claimed relation between the quantum advantage in the Gaussian QI and the quantum discord by showing their opposite behavior.

I. INTRODUCTION

Quantum illumination(QI) is a novel remote target detection technique which exploits a quantum correlation [1]. QI has a better target detection performance compared to its classical counterpart called classical-illumination(CI) with the same transmission energy under a very noisy channel [4], so after its first proposal, there have been many studies about QI [2–41].

Since quantum states exploited in QI can be written in Gaussian state form, more realistic description of QI, called the Gaussian QI, has been studied [4–8]. The Gaussian QI uses a two-mode squeezed vacuum(TMSV) state as a resource of the target detection where a TMSV state has a larger two-mode correlation compared to classically allowed. In QI, one mode of a TMSV state, called signal mode, is sent to a target for detection, and the other, idler mode, is retained ideally. The return mode from the target and the idler mode are jointly measured, and a decision is made from the measurement outcomes. To demonstrate the quantum advantage of the Gaussian QI, implementable QI receivers have been studied [9–13]. Furthermore, QI was experimentally demonstrated in laboratories not only using optical wavelengths [14–16] but also using microwave frequencies [17, 18].

Intuitively, increasing a probe power leads performance enhancement of a target detection protocol. An energy of a squeezed vacuum state is related with a squeezing parameter of squeezing operation, and thus, highly squeezed light would provide better sensitivity in QI. However, generation of a bright TMSV state needs demanding technologies. The reported mean photon number of a squeezed vacuum state is roughly 7.4 in an optical frequency [42] and one in a microwave regime [18, 19]. To overcome this technical issue, signal amplification on a generated TMSV state was studied [40]. In [40], equal amplification on the two modes was considered, and a two-mode correlation of the amplified state was analyzed to investigate a performance of the quantum-enhanced noise radar [19].

In this paper, we propose and analyze a QI protocol with asymmetrically squeezed two-mode(ASTM) light. In our QI, we independently perform single-mode squeezing operations on each mode of a generated TMSV state. By performing the squeezing operations, the mean photon number of the TMSV state is enlarged without introducing additional noise. This additional single-mode squeezing operation is implementable compared to attaining a bright TMSV state. The performance of our QI is analyzed by using the quantum Chernoff bound used as a distinguishability measure [43, 44]. We show that the additional squeezing can improve the performance of QI and that the performance can approach that of the conventional Gaussian QI with the same probe energy under certain conditions.

Additionally, our QI provides a counterexample against the claim that the quantum discord is the resource of the quantum advantage in QI [25, 26]. It was already shown that the quantum advantages in a single-shot target detection with discrete variable cannot be characterized by the quantum discord solely [30], and we firstly report the case that the quantum advantage and the quantum discord show different behavior in the Gaussian QI.

This paper is organized as follows. In Sec. II we introduce a basic concepts of QI with an ASTM state. In Sec. III tools for analyzing performance of QI is introduced, and we compare the performance of the conventional Gaussian QI, our protocol, and the CI in various situations. The relation between the quantum advantage and the quantum discord is analyzed in Sec. IV, and finally it is summarized with discussion in Sec. V.

II. QUANTUM ILLUMINATION WITH ASYMMETRIC SQUEEZING

Fig. 1(a) shows a schematic diagram of QI which is a remote target detection protocol that exploits an entangled state. The signal mode of the entangled state is sent to target, and the idler mode is ideally retained. If a target presents, the return mode which include the reflected signal and a background thermal noise is jointly measured with the idler mode, and if there is not a tar-

* yonggi@add.re.kr

† suyong2@add.re.kr

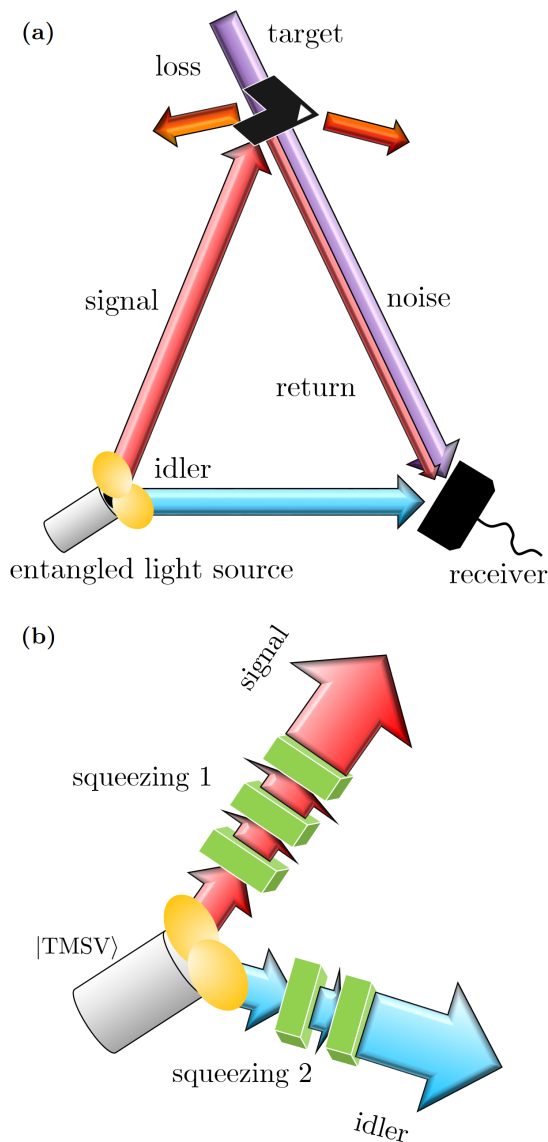


FIG. 1. (a) A schematic diagram of QI, where an entangled state is exploited to discriminate the two situations, target presence/absence. The signal mode is sent to the target, and the idler mode is retained. The return mode which includes the reflected signal and a thermal noise is jointly measured with the idler mode for decision of target existence. (b) Generation of an ASTM state, where each mode of the initial TMSV state is independently squeezed.

get, the receiver only gets the background noise and the idler mode. On the other hand, its classical counterpart exploits a single mode light to discriminate the two situations, so there is no idler mode. It was studied that the optimal CI strategy exploits a coherent state [5], and therefore a QI protocol should have lower error rate of the discrimination than the CI with the same energy to claim a quantum advantage.

A conventional Gaussian QI protocol exploits a TMSV state which is the maximally entangled state in a contin-

uous variable(CV) system. A TMSV state is written as

$$|\text{TMSV}\rangle = \sum_{n=0}^{\infty} \sqrt{\frac{(N_0)^n}{(N_0+1)^{n+1}}} |n\rangle_1 |n\rangle_2, \quad (1)$$

where N_0 is the mean photon number of each mode, and the subscripts 1 and 2 denote two different modes. Single-mode and two-mode squeezing operations are written as follows:

$$\hat{S}(z) = \exp\left[\frac{1}{2}(z^* \hat{a}^2 - z \hat{a}^{\dagger 2})\right], \quad (2)$$

$$\hat{S}'(z) = \exp\left(z^* \hat{a}_1 \hat{a}_2 - z \hat{a}_1^{\dagger} \hat{a}_2^{\dagger}\right),$$

where $z = r e^{i\phi}$ with squeezing parameter r and squeezing angle ϕ , \hat{a}^{\dagger} and \hat{a} are photon creation and annihilation operators, and the subscripts 1 and 2 mean two different modes. The mean photon number of a squeezed vacuum state and the squeezing parameter are related as $N = \sinh^2 r$ [45].

Intuitively, a strong probe signal would give better sensitivity in a remote target detection protocol. However, there is a limit to an increase of the squeezing parameter with current technologies. The squeezing parameters in the existing demonstrations are roughly $1.73(N \approx 7.41)$ in optical frequency [42] and $0.881(N \approx 1.00)$ in a microwave domain [18, 19].

We apply additional squeezing operations on a generated TMSV state to amplify the mean photon number. Fig. 1(b) shows a schematic diagram of the source for generating a two-mode state with the additional squeezing. The procedure is follows. First, a TMSV state is generated. Sequentially, a squeezing operation is performed on each mode of the TMSV state. The squeezing operations on the each mode are independent, so the result is called an asymmetrically squeezed two-mode(ASTM) state. For the mode 1 of the TMSV state, the squeezing 1($\hat{S}_1(z_1)$) is performed, and the squeezing 2($\hat{S}_2(z_2)$) is for the mode 2 of the TMSV state.

For simplification, we assume $\phi = 0$ for all additional squeezing operations. This assumption does not change the performance of QI in our analysis, since the optimal measurement is assumed in the quantum Chernoff bound, i.e., the relative squeezing angle between the signal and idler modes would be optimized at the receiver. With this assumption, it is possible to implement a squeezing operation with a large squeezing parameter by using sequential squeezing operations. A squeezing operation with a large squeezing parameter r can be performed with squeezing operations with small squeezing parameters r_a, r_b, r_c , where $r = r_a + r_b + r_c$, since $\hat{S}(r)|\text{vac}\rangle = \hat{S}(r_a)\hat{S}(r_b)\hat{S}(r_c)|\text{vac}\rangle$ satisfies where $|\text{vac}\rangle$ denotes a vacuum state. Therefore, in principle, even if there is a limitation of a squeezing parameter experimentally implementable, it is possible to construct a squeezing operation with a large squeezing parameter by using the sequential squeezing scheme.

For a calculation of Gaussian states, the quadrature representation is convenient to describe. The covariance matrix, one of the quadrature representation, of an ASTM state is obtained from the following equation:

$$\mathbf{V}_{\text{ASTM}} = \mathcal{M}_S \mathbf{V}_{\text{TMSV}} \mathcal{M}_S^T, \quad (3)$$

where the covariance matrix of a TMSV state is

$$\mathbf{V}_{\text{TMSV}} = \begin{pmatrix} A & 0 & C & 0 \\ 0 & A & 0 & -C \\ C & 0 & A & 0 \\ 0 & -C & 0 & A \end{pmatrix}, \quad (4)$$

with $A = 2N_0 + 1$ and $C = 2\sqrt{N_0(N_0 + 1)}$. The symplectic matrix \mathcal{M}_S corresponding $\hat{S}_1(r_1)\hat{S}_2(r_2)$ is written as [45]

$$\mathcal{M}_S = \begin{pmatrix} \gamma_{1-} & 0 & 0 & 0 \\ 0 & \gamma_{1+} & 0 & 0 \\ 0 & 0 & \gamma_{2-} & 0 \\ 0 & 0 & 0 & \gamma_{2+} \end{pmatrix}, \quad (5)$$

with $\gamma_{n\pm} = \sqrt{N_n + 1} \pm \sqrt{N_n}$ and $N_i = \sinh^2 r_i$. The mean photon numbers of the signal and idler modes in an ASTM state are $N_S = N_0 + 2N_0N_1 + N_1$ and $N_I = N_0 + 2N_0N_2 + N_2$, respectively. Since N_i with $i \in \{1, 2\}$ is a non-negative value, the mean photon number of the signal and idler mode is amplified from N_0 by exploiting the additional squeezing operations.

In QI, a target can be modeled by a beam splitter with the reflectivity κ . The signal mode of an ASTM state is induced one of the input ports of the beam splitter, and a thermal noise is injected the other input port. There is a receiver in one of the output ports which includes the reflected signal and transmitted thermal noise, and the other output port is discarded. The mean photon number of the thermal noise is defined as $N_B/(1 - \kappa)$, so the mean photon number of the thermal noise at the receiver is always N_B regardless of the target reflectivity. If a target exists, the covariance matrix of the return mode and the idler mode is written as follows:

$$\mathbf{V}_A = \begin{pmatrix} \sqrt{\kappa} & 0 & 0 & 0 \\ 0 & \sqrt{\kappa} & 0 & 0 \\ 0 & 0 & 1 & 0 \\ 0 & 0 & 0 & 1 \end{pmatrix} \mathbf{V}_{\text{ASTM}} \begin{pmatrix} \sqrt{\kappa} & 0 & 0 & 0 \\ 0 & \sqrt{\kappa} & 0 & 0 \\ 0 & 0 & 1 & 0 \\ 0 & 0 & 0 & 1 \end{pmatrix} + (1 - \kappa) \begin{pmatrix} 2\frac{N_B}{1-\kappa} + 1 & 0 & 0 & 0 \\ 0 & 2\frac{N_B}{1-\kappa} + 1 & 0 & 0 \\ 0 & 0 & 0 & 0 \\ 0 & 0 & 0 & 0 \end{pmatrix}, \quad (6)$$

and if there is no target ($\kappa = 0$), the covariance matrix becomes

$$\mathbf{V}_B = \begin{pmatrix} 2N_B + 1 & 0 & 0 & 0 \\ 0 & 2N_B + 1 & 0 & 0 \\ 0 & 0 & \gamma_{2-}^2 A & 0 \\ 0 & 0 & 0 & \gamma_{2+}^2 A \end{pmatrix}. \quad (7)$$

Note that the quantum states we consider, a squeezed vacuum state and a thermal state, are zero-mean Gaussian states, so that we do not need to consider the first-order moments.

III. PERFORMANCE ANALYSIS

A. Quantum Chernoff bound

Here, we provide a brief review of the quantum Chernoff bound for performance analysis of the Gaussian QI. The main problem in QI is discrimination of the two situation, target presence and target absence, and this problem is reduced to the statistical discrimination problem of two Gaussian states \mathbf{V}_A and \mathbf{V}_B . The precision limit of the problem is determined by an error probability of the decision. The probability is upper bounded by the quantum Chernoff bound, and this upper bound can be exploited as a measure of distinguishability [44].

The definition of the quantum Chernoff bound is as follows [43]:

$$P_{QC}^{(M)} = \frac{1}{2} \left[\inf_{0 \leq s \leq 1} Q_s \right]^M, \quad (8)$$

where P_{QC} is the quantum Chernoff bound, M is the number of ensembles for the decision, and

$$Q_s := \text{Tr}(\rho_A^s \rho_B^{1-s}). \quad (9)$$

The density matrices ρ_A and ρ_B are the quantum states corresponding to the covariance matrices \mathbf{V}_A and \mathbf{V}_B , respectively.

The quantum Chernoff bound for Gaussian states can be calculated from the two covariance matrices and their symplectic spectrum. For every 4×4 covariance matrix, there exists a symplectic matrix \mathbf{S} that satisfies

$$\mathbf{V} = \mathbf{S} \left[\bigoplus_{k=1}^2 \nu_k \mathbf{I}_2 \right] \mathbf{S}^T, \quad (10)$$

where ν_k is a symplectic eigenvalue and \mathbf{I}_2 denotes the 2×2 identity matrix. To describe the quantum Chernoff bound, we define the following equations:

$$\begin{aligned} G_p(x) &:= \frac{2^p}{(x+1)^p - (x-1)^p}, \\ \Lambda_p(x) &:= \frac{(x+1)^p + (x-1)^p}{(x+1)^p - (x-1)^p}, \\ \mathbf{V}(p) &:= \mathbf{S} \left[\bigoplus_{k=1}^2 \Lambda_p(\nu_k) \mathbf{I}_2 \right] \mathbf{S}^T. \end{aligned} \quad (11)$$

Then, Eq. (9) can be calculated from the following equations [46]:

$$Q_s = \tilde{Q}_s \exp \left\{ -\frac{1}{2} \vec{d}^T [\mathbf{V}_A(s) + \mathbf{V}_B(1-s)]^{-1} \vec{d} \right\}, \quad (12)$$

where

$$\tilde{Q}_s := \frac{4 \prod_{k=1}^2 G_s(\alpha_k) G_{1-s}(\beta_k)}{\sqrt{\det[\mathbf{V}_A(s) + \mathbf{V}_B(1-s)]}}. \quad (13)$$

with $\vec{d} = \vec{x}_A - \vec{x}_B$ and $\vec{x}^T := (\langle \hat{x}_R \rangle, \langle \hat{p}_R \rangle, \langle \hat{x}_I \rangle, \langle \hat{p}_I \rangle)$. The subscripts R and I denote the return and idler modes, respectively. α_k and β_k are the symplectic eigenvalues of \mathbf{V}_A and \mathbf{V}_B , so

$$\mathbf{V}_A(s) = \mathbf{S}_A \left[\bigoplus_{k=1}^2 \Lambda_s(\alpha_k) \mathbf{I}_2 \right] \mathbf{S}_A^T, \quad (14)$$

$$\mathbf{V}_B(1-s) = \mathbf{S}_B \left[\bigoplus_{k=1}^2 \Lambda_{1-s}(\beta_k) \mathbf{I}_2 \right] \mathbf{S}_B^T. \quad (15)$$

In our Gaussian QI, $Q_s = \tilde{Q}_s$ always satisfies, since the quantum states we consider are zero-mean Gaussian states.

Here, for simplicity, we analyze performance of QI by using the signal-to-noise ratio (SNR) rather than comparing error probabilities. The relation between SNR and the error probability is written in the following equation [12, 13, 18]:

$$P_{QC}^{(M)} = \frac{1}{2} \operatorname{erfc} \left[\sqrt{\operatorname{SNR}_{QC}^{(M)}} \right], \quad (16)$$

where erfc is the complementary error function. Hereafter, we omit the subscript QC and the superscript (M) , but all the SNRs in plots and equations mean $\operatorname{SNR}_{QC}^{(M)}$.

B. Performance improvement in quantum illumination with asymmetric squeezing

In this section, we analyze the performance of the Gaussian QI by using the SNR. First, we analyze the effect of additional squeezing operations on the each mode of the initial TMSV state. We consider a situation of the microwave QI [6, 18] since the recorded squeezing parameter of a TMSV state is smaller than that in an optical frequency. We set the mean photon number of the initial TMSV state as $N_0 = 1$ [19] and the energy of the thermal noise as $N_B = 3.8 \times 10^3$ that corresponds to a thermal radiation of a few GHz frequency at the room temperature. Reflectivity of the target is fixed as $\kappa = 0.01$, and the number of ensembles is $M = 10^7$.

Fig. 2(a) shows the case that the idler mode energy $N_I = N_0 + 2N_0N_2 + N_2$ is amplified from N_0 by performing the additional squeezing operation N_2 . The red dashed line denotes the SNR when there is no additional squeezing on the signal mode ($N_S = N_0 = 1$), and the black line does the SNR with the squeezed signal mode from $N_0 = 1$ to $N_S = 2$. Both plots are not changed with varying N_I , and thus we can conclude that the SNR is not affected by the additional squeezing operation on the idler mode.

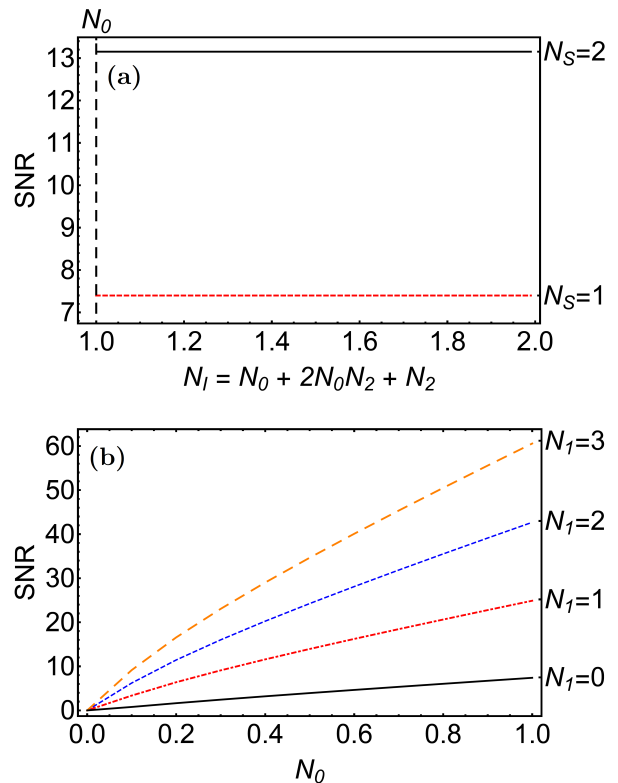


FIG. 2. (a) Given a fixed signal mode N_S , SNR as a function of the idler mode $N_I = N_0 + 2N_0N_2 + N_2$, where N_2 corresponds to the squeezing parameter of the single-mode squeezing operation on the idler mode. The red dashed line denotes the case there is no squeezing on the signal mode ($N_S = N_0 = 1$), and the black line does the case with the squeezed signal mode $N_S = 2$. (b) Given a fixed idler mode $N_I = N_0$, SNR as a function of the signal mode of the initial TMSV state N_0 with the various squeezing parameter N_1 . The parameter values in the plots are $N_0 = 1$, $N_B = 3.8 \times 10^3$, $\kappa = 0.01$, and $M = 10^7$.

The reason that the additional squeezing on the idler mode does not affect SNR of QI is follows. Here, as already described, we analyze the performance of QI by using the quantum Chernoff bound, and the quantum Chernoff bound includes the assumption of the optimal measurement. The idler mode is ideally retained and jointly measured with the return mode, and thus, it is possible to perform any additional single-mode operation on the idler mode before the measurement. This means that if the additional squeezing operation on the idler mode can improve the performance of QI, it is already considered in the calculation of the quantum Chernoff bound in the conventional Gaussian QI. Therefore, an additional squeezing on the idler mode does not affect SNR based on the quantum Chernoff bound.

In Fig. 2(b), SNRs of QI with a TMSV state and ASTM states with various squeezing parameter N_1 are shown against the energy of the initial TMSV state. Recall that the signal mode energy of an ASTM state is

given by $N_S = N_0 + 2N_0N_1 + N_1$, and the experimentally reported squeezing parameter is $N \approx 1$ in a microwave frequency [19]. The SNR of QI is roughly 7 with the TMSV state $N_S = N_0 = 1$, and it is improved to roughly 25 with the additional squeezing on the signal mode $N_1 = 1$. SNR can be more improved by using the sequential squeezing shown in Fig. 1(b), and it becomes roughly 43 and 61 with the additional squeezing operations with $N_1 = 2$ and $N_1 = 3$, respectively. From the result, we can claim that the additional single-mode squeezing on the signal mode provides a significant improvement in the Gaussian QI.

In the Gaussian QI, the cross-correlation terms, $\langle \hat{a}_R \hat{a}_I \rangle$ and $\langle \hat{a}_R^\dagger \hat{a}_I^\dagger \rangle$, are exploited to detect a target where \hat{a}^\dagger and \hat{a} are creation and annihilation operators [9, 13]. The single-mode squeezing operation on the signal mode amplifies not only the energy of the signal mode, from N_0 to $N_0 + 2N_0N_1 + N_1$, but also the cross-correlation, from $\sqrt{N_0(N_0 + 1)}$ to $\sqrt{N_0(N_0 + 1)(N_1 + 1)}$. These enlarged probe energy and cross-correlation lead the performance improvement in the Gaussian QI.

In Fig. 3, the performance of QI with a TMSV state and that with an ASTM state are compared at the same transmitted energy as well. As a benchmark, SNR of CI using a coherent state with the same probe energy is plotted. QI should have better SNR than the CI for quantum advantage. The signal energies of a TMSV state, a coherent state, and an ASTM state are $N_S = N_0$, $N_S = |\alpha|^2$, and $N_S = N_0 + 2N_0N_1 + N_1$, respectively. The ASTM state is generated from the initial TMSV state with $N_0 = 1$. Since we already showed a squeezing on the idler mode does not change the performance of QI, only the signal mode is additionally squeezed. The other conditions are the same to those used in Fig. 2.

In Fig. 3(a), QI with an ASTM state has better performance compared to the CI, and SNR of QI with an ASTM state approaches that of the conventional Gaussian QI with the same probe energy. For example, in the plots, the SNR of our protocol is 93.8% at $N_S = 2$ and 91.9% at $N_S = 4$ of the SNR of QI using a TMSV state with the same energy. The ratio between the two SNRs is larger than 90% in the plotted regime, while our QI protocol is implementable compared to generating a bright TMSV state. Fig. 3(b) shows the SNRs as a function of reflectivity of the target. In the plot, the signal mode energy is fixed as $N_S = 2$ for all the states, and the initial TMSV state for an ASTM state has $N_0 = 1$. The plot shows SNR of QI with an ASTM state is similar to that of QI using TMSV state with the same energy, for example, the ratio at $\kappa = 0.05$ is 93.4%. Therefore, if there is short of a bright TMSV state, we can replace it by the ASTM state with the same probe energy.

C. Conditions for quantum advantage

Here, we show that the quantum advantage of QI is not always obtained with an energy amplified probe in QI. In

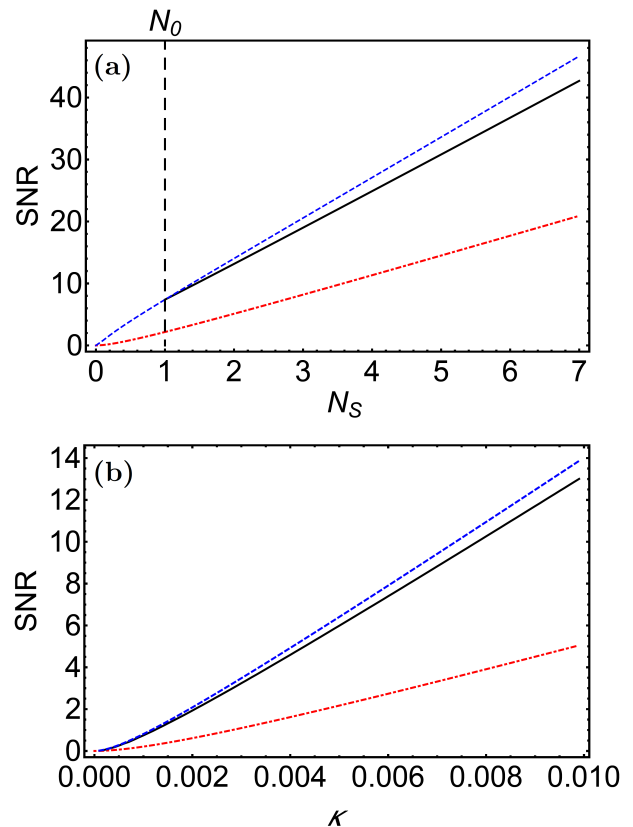


FIG. 3. SNR using a TMSV state ($N_S = N_0$, blue dashed lines), a coherent state ($N_S = |\alpha|^2$, red dot-dashed lines), and an ASTM state ($N_S = N_0 + 2N_0N_1 + N_1$, black lines). (a) Given a fixed target reflectivity $\kappa = 0.01$, SNR as a function of the total input energy in the signal mode N_S . (b) Given a fixed $N_S = 2$, SNR as a function of the target reflectivity κ . The initial TMSV state has $N_0 = 1$ for generating the ASTM state.

the previous section, we showed QI with an ASTM state has better performance than the CI in Fig. 3. However, we find the case that QI with an ASTM state has lower SNR than the CI with the same probe energy, and it is shown in Fig. 4. In this plot, we choose the parameter values as $N_B = 30$, $\kappa = 0.01$, and $M = 10^7$. Energy of the initial TMSV state for generating an ASTM state is $N_0 = 0.1$. Different from Fig. 3(a), in Fig. 4, the slope of SNR of QI with an ASTM state is smaller than that of the CI, and thus, QI with an ASTM state becomes inferior compared to the CI with increasing N_S .

We find that the slope of SNR of QI with an ASTM state as a function of N_S mainly depends on the squeezing parameter of the initial TMSV state rather than other parameters. We approximate the SNRs in Fig. 4(a) as a linear functions for the slope analysis. Fig. 4(b) shows the slope of the SNRs as a function of the mean photon number of the initial TMSV state N_0 . If this slope is equal to or larger than that of the CI, QI with an ASTM always has better performance compared to the CI. Therefore, the initial TMSV state should have enough energy to

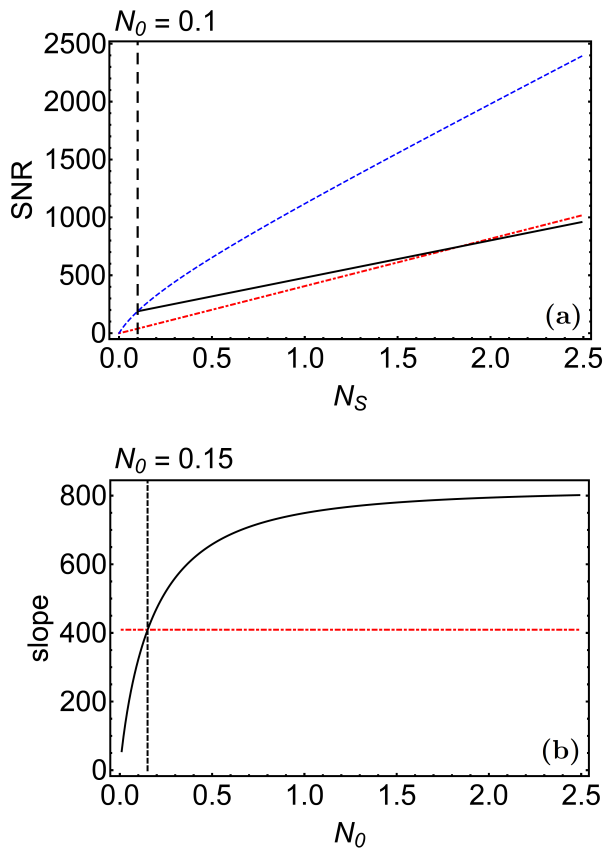


FIG. 4. (a) SNR as a function of the total input energy in the signal mode. The energy is $N_S = N_0$ for a TMSV state (blue dashed line), $N_S = |\alpha|^2$ for a coherent state (red dot-dashed line), and $N_S = N_0 + 2N_0N_1 + N_1$ for an ASTM state (black line) where $N_0 = 0.1$ is the energy of the initial ASTM state. (b) Approximated slope of the SNR as a function of the initial input energy in the signal mode N_0 (black line). The red dot-dashed line denotes the slope of the CI.

construct an efficient QI protocol with an ASTM state, and the value in our situation is $N_0 \geq 0.15$.

IV. QUANTUM ADVANTAGE OF GAUSSIAN QUANTUM ILLUMINATION AND QUANTUM DISCORD

Many quantum information protocols exploit superposition and entanglement such as quantum communication [47, 48] and quantum computing [49]. In these protocols, protecting the quantum phenomena against decoherence is very crucial issue. Different from other quantum information protocols, QI shows advantages compared to the CI even when entanglement is not left after passing through the channel. Thus, there have been many studies to investigate the origin of quantum advantage of QI. It was claimed that the quantum discord is the resource of the quantum advantage in QI using discrete variables [25] and in the Gaussian QI [26], since the quan-

tum discord is a measure of nonclassical correlation beyond entanglement [50–52]. However, it was shown that the quantum discord cannot fully characterize the quantum advantages in QI with discrete signals [30]. Here, we firstly show a counterexample of the relation between the quantum advantages in the Gaussian QI and the quantum discord.

We start from the covariance matrix of a two-mode Gaussian state:

$$\mathbf{V} = \begin{pmatrix} V_{11} & V_{12} \\ V_{21} & V_{22} \end{pmatrix}, \quad (17)$$

where V_{ij} is a 2×2 block matrix, and we define $\alpha := \text{Det}[V_{11}]$, $\beta := \text{Det}[V_{22}]$, $\gamma := \text{Det}[V_{12}] = \text{Det}[V_{21}]$, and $\delta := \text{Det}[\mathbf{V}]$. Then the quantum discord for a Gaussian two-mode state can be calculated from the following equation [53, 54]:

$$\tilde{\mathcal{D}} = f(\sqrt{\beta}) - f(\sqrt{\nu_-}) - f(\sqrt{\nu_+}) + f(\sqrt{\epsilon}), \quad (18)$$

where

$$f(x) = \frac{x+1}{2} \ln \frac{x+1}{2} - \frac{x-1}{2} \ln \frac{x-1}{2}, \quad (19)$$

$$\nu_{\pm} = \alpha + \beta + 2\gamma \pm \sqrt{\frac{(\alpha + \beta + 2\gamma)^2 - 4\delta}{2}}, \quad (20)$$

and if $(\delta - \alpha\beta)^2 \leq (\beta + 1)\gamma^2(\alpha + \delta)$

$$\epsilon = \frac{2\gamma^2 + (\beta - 1)(\delta - \alpha) + 2|\gamma|\sqrt{\gamma^2 + (\beta - 1)(\delta - \alpha)}}{(\beta - 1)^2}, \quad (21)$$

otherwise

$$\epsilon = \frac{\alpha\beta - \gamma^2 + \delta - \sqrt{\gamma^4 + (\delta - \alpha\beta)^2 - 2\gamma^2(\delta + \alpha\beta)}}{2\beta}. \quad (22)$$

In Eqs. (18–22), the quantum discord is calculated from the determinants of the block matrices of the covariance matrix. The additional squeezing operations for generating an ASTM state are local operations, so they do not change the determinants. Thus, the quantum discord of the initial TMSV state and that of the generated ASTM state are the same. However, we find that the remained quantum discord after the channel, i.e., the quantum discord between the return and idler modes, is changed with the varying squeezing parameters. Here, we analyze the remained quantum discord and the performance of QI.

Fig. 5(a) shows the quantum advantage of our QI compared to the CI. The quantum advantage is calculated from (SNR of QI with an ASTM state)/(SNR of the CI with the same energy), where the both SNRs are already shown in Fig. 4(a). The quantum advantage is a monotonic function with increasing N_S , but compared to this, in as shown in Fig. 5(b), the quantum discord between the return and idler modes is not a monotonic function of

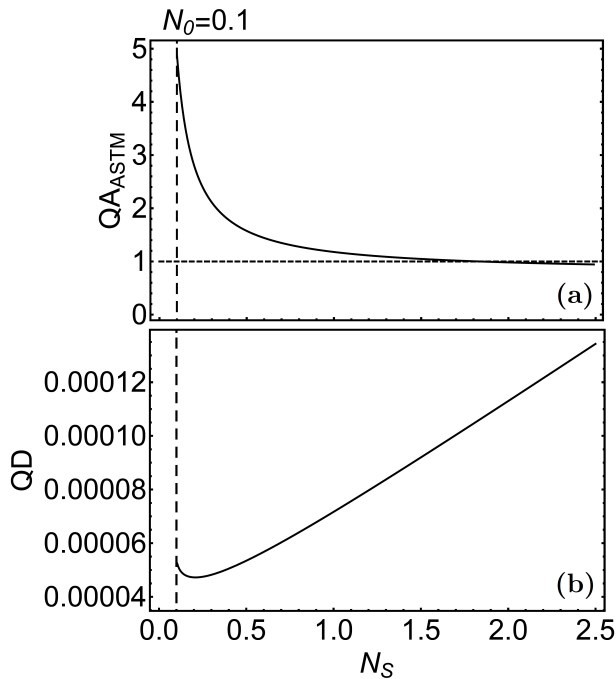


FIG. 5. (a) Quantum advantage(QA) of QI using an ASTM state over the CI as a function of the total input energy in the signal mode $N_S = N_0 + 2N_0N_1 + N_1$. (b) Quantum discord(QD) between the return and idler modes of the ASTM state as a function of N_S . The parameter values are the same as those of Fig. 4(a).

N_S . The functional form of the quantum discord is different from not only the quantum advantage but also the SNR of our QI. Moreover, the quantum advantage monotonically decreases with increasing N_S , while the quan-

tum discord increases at large N_S , i.e., the two quantities show opposite behavior at large N_S . Therefore, we can claim that the quantum discord cannot be the resource of the quantum advantage in the Gaussian QI as well as it cannot in QI with a discrete signal [30].

V. SUMMARY AND DISCUSSION

We proposed a QI protocol using asymmetrically squeezed two-mode light. By applying single-mode squeezing operations on the initial TMSV state, the mean photon number in the each mode is amplified. We found that the squeezing on the signal mode which interacts with a target can improve the performance of the Gaussian QI, while squeezing on the idler mode has no effect. Moreover, the performance of our protocol is comparable to that of QI using a TMSV state with the same probe energy under certain conditions. We found the condition to construct efficient QI with an ASTM state that is related to the energy of the initial TMSV state which can be fulfilled with the amount of squeezing in the existing demonstrations [19, 42]. This result provides a theoretical platform for a practical and efficient QI, since generation of a bright TMSV state needs demanding technologies. Finally, we show that the quantum discord cannot be the resource of the quantum advantage in the Gaussian QI by showing their opposite behaviors.

ACKNOWLEDGMENTS

This work was supported by a grant to the Quantum Standoff Sensing Defense-Specialized Project funded by the Defense Acquisition Program Administration and the Agency for Defense Development.

-
- [1] S. Lloyd, *Science* **321**, pp. 1463–1465 (2008).
 - [2] J. Shapiro, *IEEE Aerospace and Electronic Systems Magazine* **35**(4), pp. 8–20 (2020).
 - [3] D. Luong, S. Rajan, and B. Balaji, *IEEE Aerospace and Electronic Systems Magazine* **35**(4), pp. 22–35 (2020).
 - [4] S. Tan, B. Erkmen, V. Giovannetti, S. Guha, S. Lloyd, L. Maccone, S. Pirandola, and J. Shapiro, *Phys. Rev. Lett.* **101**, 253601 (2008).
 - [5] J. H. Shapiro and S. Lloyd, *New J. Phys.* **11**, 063045 (2009).
 - [6] S. Barzanjeh, S. Guha, C. Weedbrook, D. Vitali, J. Shapiro, and S. Pirandola, *Phys. Rev. Lett.* **114**, 080503 (2015).
 - [7] M. M. Wilde, M. Tomamichel, S. Lloyd, and M. Berta, *Phys. Rev. Lett.* **119**, 120501 (2017).
 - [8] A. Karsa, G. Spedalieri, Q. Zhuang, and S. Pirandola, *Phys. Rev. Res.* **2**, 023414 (2020).
 - [9] S. Guha and B. Erkmen, *Phys. Rev. A* **80**, 052310 (2009).
 - [10] S. Guha, 2009 IEEE International Symposium on Information Theory, Seoul, pp. 963–967 (2009).
 - [11] Q. Zhuang, Z. Zhang, and J. Shapiro, *Phys. Rev. Lett.* **118**, 040801 (2017).
 - [12] A. Karsa and S. Pirandola, *IEEE Aerospace and Electronic Systems Magazine* **35**(11), pp. 22–29 (2020).
 - [13] Y. Jo, S. Lee, Y. S. Ihn, Z. Kim, and S.-Y. Lee, *Phys. Rev. Res.* **3**, 013006 (2021).
 - [14] E. Lopaeva, I. Berchera, I. Degiovanni, S. Olivares, G. Brida, and M. Genovese, *Phys. Rev. Lett.* **110**, 153603 (2013).
 - [15] Z. Zhang, S. Mouradian, F. Wong, and J. Shapiro, *Phys. Rev. Lett.* **114**, 110506 (2015).
 - [16] D. England, B. Balaji, and B. Sussman, *Phys. Rev. A* **99**, 023828 (2019).
 - [17] D. Luong, C. W. Sandbo Chang, A. M. Vadiraj, A. Damini, C. M. Wilson, and B. Balaji, *IEEE Transactions on Aerospace and Electronic Systems* **56**(3), pp. 2041–2060 (2020).
 - [18] S. Barzanjeh, S. Pirandola, D. Vitali, and J. Fink, *Sci. Adv.* **6**, eabb0451 (2020).

- [19] C. W. Sandbo Chang, A. M. Vadiraj, J. Bourassa, B. Balaji, and C. M. Wilson, *Appl. Phys. Lett.* **114**, 112601 (2019).
- [20] A. R. Usha Devi and A. K. Rajagopal, *Phys. Rev. A* **79**, 062320 (2009).
- [21] S. Ragy, I. Ruo Berchera, I. P. Degiovanni, S. Olivares, M. G. A. Paris, G. Adesso, and M. Genovese, *J. Opt. Soc. Am. B* **31**, 2045 (2014).
- [22] S. L. Zhang, J. S. Guo, W. S. Bao, J. H. Shi, C. H. Jin, X. B. Zou, and G. C. Guo, *Phys. Rev. A* **89**, 062309 (2014).
- [23] M. Sanz, U. Las Heras, J. J. García-Ripoll, E. Solano, and R. Di Candia, *Phys. Rev. Lett.* **118**, 070803 (2017).
- [24] K. Liu, Q.-W. Zhang, Y.-J. Gu, and Q.-L. Li, *Phys. Rev. A* **95**, 042317 (2017).
- [25] C. Weedbrook, S. Pirandola, J. Thompson, V. Vedral, and M. Gu, *New. J. Phys.* **18**, 043027 (2016).
- [26] M. Bradshaw, S. M. Assad, J. Y. Haw, S.-H. Tan, P. K. Lam, and M. Gu, *Phys. Rev. A* **95**, 022333 (2017).
- [27] L. Fan and M. S. Zubairy, *Phys. Rev. A* **98**, 012319 (2018).
- [28] S. Pirandola, R. Laurenza, C. Lupo, and J. L. Pereira, *npj Quantum Inf.* **5**, 50 (2019).
- [29] G. De Palma and J. Borregaard, *Phys. Rev. A* **98**, 012101 (2018).
- [30] M. H. Yung, F. Meng, X.-M. Zhang, and M.-J. Zhao, *npj Quantum Inf.* **6**, 75 (2020).
- [31] S. Ray, J. Schneeloch, C. C. Tison, and P. M. Alsing, *Phys. Rev. A* **100**, 012327 (2019).
- [32] W.-Z. Zhang, Y.-H. Ma, J.-F. Chen, and C.-P. Sun, *New J. Phys.* **22**, 013011 (2020).
- [33] R. Nair and M. Gu, *Optica* **7**, 771 (2020).
- [34] G. H. Aguilar, M. A. de Souza, R. M. Gomes, J. Thompson, M. Gu, L. C. Céleri, and S. P. Walborn, *Phys. Rev. A* **99**, 053813 (2019).
- [35] Y. Zhang, D. England, A. Nomerotski, P. Svihra, S. Ferrante, P. Hockett, and B. Sussman, *Phys. Rev. A* **101**, 053808 (2020).
- [36] S.-Y. Lee, Y. S. Ihn, and Z. Kim, *Phys. Rev. A* **103**, 012411 (2021).
- [37] F. Daum, *IEEE Aerospace and Electronic Systems Magazine* **35**(11), pp. 8–20 (2020).
- [38] M. Lanzagorta and J. Uhlmann, *IEEE Aerospace and Electronic Systems Magazine* **35**(11), pp. 38–56 (2020).
- [39] J. Bourassa and C. M. Wilson, *IEEE Aerospace and Electronic Systems Magazine* **35**(11), pp. 58–69 (2020).
- [40] J. Bourassa and C. M. Wilson, *2020 IEEE International Radar Conference (RADAR)* (Washington, DC, USA, 2020), pp. 973–978.
- [41] J. N. Blakely, arXiv:2103.09757 [quant-ph] (2021).
- [42] H. Vahlbruch, M. Mehmet, K. Danzmann, and R. Schnabel, *Phys. Rev. Lett.* **117**, 110801 (2016).
- [43] K. Audenaert, J. Calsamiglia, R. Muñoz-Tapia, E. Bagan, L. Masanes, A. Acín, and F. Verstraete, *Phys. Rev. Lett.* **98**, 160501 (2007).
- [44] J. Calsamiglia, R. Muñoz-Tapia, L. Masanes, A. Acín, and E. Bagan, *Phys. Rev. A* **77**, 032311 (2008).
- [45] C. Weedbrook, S. Pirandola, R. García-Patrón, N. J. Cerf, T. C. Ralph, J. H. Shapiro, and S. Lloyd, *Rev. Mod. Phys.* **84**, pp. 621–669 (2012).
- [46] S. Pirandola and S. Lloyd, *Phys. Rev. A* **78**, 012331 (2008).
- [47] C. Bennett and G. Brassard, In *Proceedings of the IEEE International Conference on Computers, Systems and Signal Processing* (IEEE, 1984), pp. 175–179.
- [48] A. Ekert, *Phys. Rev. Lett.* **67**, pp. 661–663 (1991).
- [49] R. Feynman, *Int. J. Theor. Phys.* **21**, pp. 467–488 (1982).
- [50] H. Ollivier and W. H. Zurek, *Phys. Rev. Lett.* **88**, 017901 (2001).
- [51] L. Henderson and V. Vedral, *J. Phys. A: Math. Gen.* **34**, 6899 (2001).
- [52] K. Modi, A. Brodutch, H. Cable, T. Paterek, and V. Vedral, *Rev. Mod. Phys.* **84**, 1655 (2012).
- [53] P. Giorda and M. G. A. Paris, *Phys. Rev. Lett.* **105**, 020503 (2010).
- [54] G. Adesso and A. Datta, *Phys. Rev. Lett.* **105**, 030501 (2010).